Hepatology Research

Hepatology Research 2018; **48**: 1008–1019 doi: 10.1111/hepr.13205

Original Article

Dual-energy computed tomography for non-invasive staging of liver fibrosis: Accuracy of iodine density measurements from contrast-enhanced data

Keitaro Sofue,[1,2] Masakatsu Tsurusaki,[1] Achille Mileto,[3] Tomoko Hyodo,[1] Kosuke Sasaki,[4] Tatsuya Nishii,[2] Takaaki Chikugo,[5] Norihisa Yada,[6] Masatoshi Kudo,[6] Kazuro Sugimura[2] and Takamichi Murakami[1]

Departments of [1]Radiology, and [5]Pathology, Kindai University Faculty of Medicine, Osaka-Sayama, [2]Department of Radiology, Kobe University Graduate School of Medicine, Kobe, [4]CT Research Group, GE Healthcare Japan, Hino, [6]Department of Gastroenterology and Hepatology, Kindai University Faculty of Medicine, Osaka, Japan and [3]Department of Radiology, University of Washington School of Medicine, Seattle, Washington, USA

Aim: To investigate whether iodine density measurements from contrast-enhanced dual-energy computed tomography (CT) data can non-invasively stage liver fibrosis.

Methods: This single-center, prospective study was approved by our IRB with written informed consent. Forty-seven consecutive patients (26 men and 21 women; mean age, 63.1 years) with chronic liver disease underwent contrast-enhanced dual-energy CT of the liver (non-contrast, arterial, portal venous, and equilibrium phase images), followed by liver biopsy. Iodine density of liver and aorta were obtained by two independent observers. Iodine uptake of the liver (Δ Liver), representing the difference in iodine density between equilibrium phase and non-contrast images, was calculated and normalized by aorta (Δ Liver/Aorta). We accounted for contrast agent distribution volume by using hematocrit level. Accuracy of iodine density measurements for staging liver fibrosis was assessed by using receiver operating characteristic (ROC) curves. Multivariate linear regression analysis was used to assess the impact of independent variables (liver fibrosis stage and patient-related confounders) on iodine uptake.

Results: The Δ Liver/Aorta significantly increased and moderately correlated with METAVIR liver fibrosis stage ($\rho = 0.645$, $P < 0.001$). Areas under the ROC curve ranged from 0.795 to 0.855 for discriminating each liver fibrosis score (≥F1–F4). METAVIR fibrosis stage was the most significant independent factor associated with Δ Liver ($P = 0.005$) and Δ Liver/Aorta ($P < 0.001$).

Conclusion: Hepatic extracellular volume fraction with contrast-enhanced dual-energy CT can non-invasively stage liver fibrosis in chronic liver diseases. This technique could prove useful for monitoring disease progression and treatment response, potentially reducing the need for liver biopsy.

Key words: dual-energy CT, fibrosis, iodine, liver, quantification

INTRODUCTION

CHRONIC LIVER DISEASES represent the leading cause of liver-related morbidity and mortality and have become a serious public health concern.[1] Sustained inflammation of the liver leads to diffuse interstitial fibrosis with expansion of the extracellular space by collagenous deposition. Progressive liver fibrosis eventually leads to cirrhosis with increased risk for hepatocellular carcinoma.[2–4] Accurate staging of liver fibrosis is of paramount importance for optimizing patient management, guiding therapeutic strategies, and predicting prognosis. Although core biopsy represents the current gold standard for assessment of liver fibrosis, it has several drawbacks including invasiveness, observer dependence, and potential for sampling errors.[5–7] Development of non-invasive techniques for staging liver fibrosis is therefore highly desirable.

A variety of imaging techniques, including ultrasonography (US), magnetic resonance (MR) imaging, and morphometric analysis, are clinically used for staging

Correspondence: Dr Keitaro Sofue, Assistant professor of Radiology, Kobe University Graduate School of Medicine, 7-5-2, Kusunoki-cho, Chuo-ku, Kobe, 650-0017, Japan. Email: keitarosofue@gmail.com

Conflict of interest: K.S., M.T., A.M., T.H., T.N., T.C., N.Y., M.K., K.S., and T.M., have no conflict of interest. K.S. is employee of GE Healthcare.

Financial support: None declared.

Received 12 January 2018; revision 7 June 2018; accepted 6 July 2018.

of liver fibrosis.[8–11] Use of computed tomography (CT) with measurement of hepatic extracellular volume (ECV) fraction on equilibrium phase images has also been advocated for estimation of liver fibrosis.[12–15] Nevertheless, clinical adoption of hepatic ECV fraction CT protocols has been dampened by requirements of longer scanner usage time (i.e., 5–10 min after administration of contrast agent) as well as the necessity for larger amounts of contrast media.[12,13]

Burgeoning evidence supports adoption of dual-energy CT to obtain material-specific information in abdominal imaging.[16–18] Projection data from a dual-energy CT acquisition can be decomposed into material basis pairs, such as iodine and water, and iodine density images can be used to quantify tissue iodine concentration.[19–21] No studies have evaluated the utility of iodine density measurements for staging liver fibrosis. We hypothesized that iodine density measurements from dual-energy contrast-enhanced data can accurately capture different degrees of liver fibrosis, thus potentially serving as desirable quantitative imaging-based biomarkers for non-invasive staging and disease monitoring.

The purpose of our study was to investigate whether iodine density measurements from contrast-enhanced dual-energy CT data can non-invasively stage liver fibrosis.

METHODS

THIS PROSPECTIVE STUDY was approved by our institutional review board. Written informed consent was obtained from all patients. One author (K.S.) is an employee of (GE Healthcare). The authors who are not consultants for industry had control of inclusion of any data and information that might present a conflict of interest for (GE Healthcare). The authors did not receive industry support specifically for this study.

Study population

For this study, we prospectively recruited consecutive patients with chronic liver disease who were referred for clinically indicated multiphase liver CT followed by biopsy, during a 15-month study period. Study inclusion criteria were: (i) age >18 years and (ii) clinical suspicion of liver disease or known chronic liver disease. Study exclusion criteria were: (i) contraindication to contrast-enhanced CT (iodinated contrast agent allergy and estimated glomerular filtration rate <60 mL/min/1.73 m^2); (ii) breast feeding or pregnancy; and (iii) liver biopsy specimen yielding less than six portal tracts (except for cirrhosis).

Patient demographic data were collected from electronic medical records. The serum hematocrit level in each patient was obtained on the same day 6 h before CT examination. In the setting of a prospectively designed clinical study, patient characteristics and an accrual process flowchart are presented in the "Results" section.

Histological analysis

Ultrasound-guided percutaneous core liver biopsy was carried out as part of patients' clinical standard of care by a single hepatologist (N.Y. with 14 years of experience in liver biopsy). For each patient, two cores of liver tissue were obtained from the right hepatic lobe (i.e., segments V/VIII) by using the Tru-Cut technique with an 18-G needle. To minimize sampling error and interobserver variability, repeat biopsy was carried out when biopsy specimens were <10 mm long.[7] The biopsy specimens were fixed in formalin and embedded in paraffin; 4-mm-thick slices were stained with hematoxylin–eosin and Masson's trichrome. If the specimen contained less than six portal tracts (except for cirrhosis), patients were excluded from the study. All specimens were interpreted by at least two pathologists by consensus (one co-author T.C. with 30 years of experience), who were blinded to imaging results and patient data. Liver fibrosis was staged using a five-point scale according to the METAVIR scoring system: F0, no fibrosis; F1, portal fibrosis without septa; F2, portal fibrosis and few septa; F3, numerous septa without cirrhosis; and F4, cirrhosis.[22] The necroinflammatory activity grade was also scored on a four-point scale: A0, no activity; A1, mild activity; A2, moderate activity; and A3, severe activity.[22]

Computed tomography examination

All CT examinations were acquired using a single-source, 64-section multidetector dual-energy CT scanner with fast kV switching (Discovery CT 750 HD; GE Healthcare, Waukesha, WI, USA). Subjects were scanned in a feet-first position on the scanning couch. Once anterior–posterior and mediolateral topograms were obtained, a multiphase hepatic CT study of the liver was acquired in dual-energy mode. Of note, after acquisition of non-contrast images, contrast-enhanced images were obtained at 25–40 s (i.e., arterial phase with bolus tracking technique), 70 s (portal venous phase), and 180 s (equilibrium phase) after contrast administration. Arterial phase images were scanned 6 s after the CT attenuation value in the region of interest in the abdominal aorta reached a peak plateau. An iodinated non-ionic contrast agent (iohexol 300 mgI/mL; Daiichi Sankyo, Tokyo, Japan, or iopamidol 370 mgI/mL; Bayer Yakuhin, Osaka, Japan) was injected through a 20-G i.v. angiocatheter in the patient's antecubital fossa or forearm, by using a dual-chamber

mechanical power injector at a dose of 600 mgI/kg of patient body weight and a fixed duration of 30 s. All acquisitions, including the non-contrast scan, were obtained in dual-energy mode (Gemstone Spectral Imaging [GSI]; GE Healthcare) using the following parameters: tube voltages, 80/140 kVp; tube current, 640 mAs; rotation speed, 0.6 s; helical pitch, 1.375; detector collimation, 0.625 mm × 64; and volume CT dose index, 15.64 mGy with mean dose length product of 498 ± 51 mGy-cm (range, 434–636 mGy-cm).

Image reconstruction

Iodine density images were obtained by using 5-mm section collimation with a projection-based material-decomposition algorithm. Projection data from non-contrast, late hepatic arterial, portal venous, and equilibrium phase images were networked to an offline workstation (AW VolumeShare5; GE Healthcare) for review and further post-processing. First, 70 keV of virtual monochromatic images with 5-mm thickness and standard kernel were reconstructed from dual-energy calculation of low- and high-energy projection data by using a two-material decomposition algorithm with the iodine–water material basis pair available on the GSI. Iodine density images on non-contrast, late hepatic arterial, portal venous, and equilibrium phase were obtained on dual energy CT dedicated analysis software (GSI Viewer; GE Healthcare). Material density images represent the relative densities in each material basis pair and the values obtained on material density images reflect the proportion or relative quantity of material under investigation.[21] Considering iodine/water binary material assortments, the effective iodine density image is represented by the iodine–water dataset. Each voxel is decomposed proportionally into the iodine–water material basis pair per the attenuation characteristics of that voxel as measured at each energy level (80 and 140 kV). A region of interest (ROI) measurement from an iodine density image estimates the relative effective density of iodine without water (mg/cm^3).[21]

Image analysis

Dual-energy iodine density measurements were independently obtained by two board-certified abdominal radiologists (K.S. and M.T. with 15 and 22 years of experience, respectively), who were blinded to histopathologic findings and patient clinical outcome. All measurements were obtained on transverse iodine density images on a dedicated dual-energy workstation (GSI Viewer; GE Healthcare). Prior to beginning of image analysis, we held a training session during which readers were shown three cases under instruction of a supervisor who was not involved in subsequent readouts.

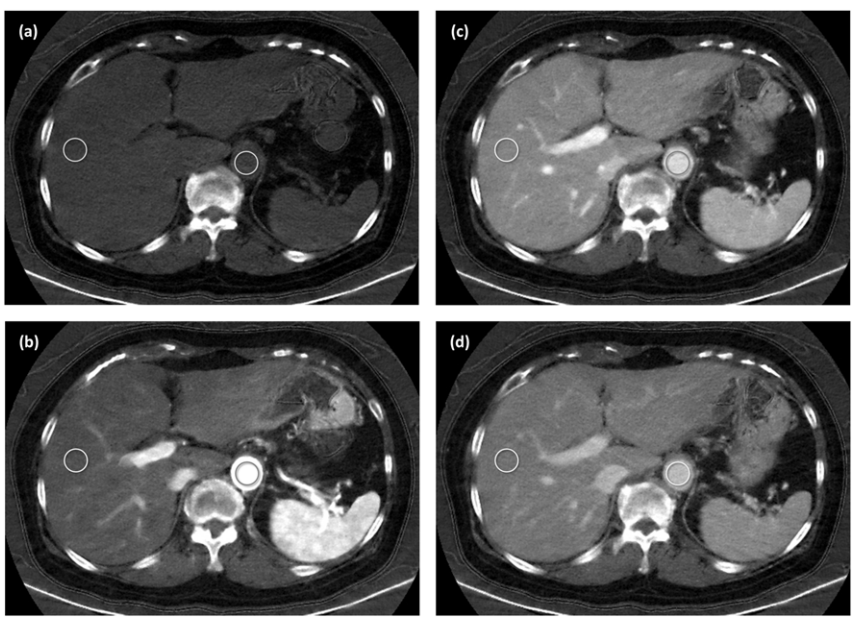

Figure 1 Transverse contrast-enhanced dual-energy iodine density images obtained in a 46-year-old man with chronic hepatitis B infection. (a) Non-contrast. (b) Arterial phase. (c) Portal venous phase. (d) Equilibrium phase images. Regions of interest (circled) were manually drawn on the liver and aorta.

For each patient, iodine density images from non-contrast, late hepatic arterial phase, portal venous, and equilibrium phases were displayed side-by-side with a manually adjustable soft-tissue window (Fig. 1). Mean iodine density values (mg/cm^3) from liver and aorta were collected by manually placing ROIs at the same image level. Iodine density from the liver was recorded by placing 100-mm^2 round ROIs in the segment V–VIII, where liver biopsy specimens were obtained. Focal lesions, areas of focal changes in parenchymal density, large vessels, and visible artifacts, if any, were carefully avoided. Iodine density from aorta was recorded using 100-mm^2 round ROIs that were as large as the vessel lumen, by carefully avoiding calcifications or mural thrombus. For all ROI measurements, size, shape, and position were kept constant among the four phases and visually colocalized ROIs in each phase at the workstation. To ensure consistency and reproducibility of data, all measurements were carried out three times at the level of the main portal vein on three consecutive images, and mean values were calculated.

Based on previous studies evaluating liver fibrosis,[12–14,23] liver fibrosis was calculated as liver density normalized by vessels (i.e., aorta and portal vein). Additionally, the volume of contrast agent is thought to be distributed as 1 − hematocrit.[12–14] We therefore examined two parameters to estimate iodine uptake of the liver, referred to as "Δ Liver", which represented the difference in iodine density between equilibrium phase and non-contrast images. Arterial and portal phase images were mainly used to avoid areas of focal changes in parenchymal density and large vessels in the liver parenchyma. Δ Liver was then normalized by the aorta by using the following equations:

$$\Delta\,\mathrm{Liver} = \mathrm{Liver}_{\mathrm{EP}} - \mathrm{Liver}_{\mathrm{pre}}$$

$$\Delta\,\mathrm{Liver/Aorta} = \left(\mathrm{Liver}_{\mathrm{EP}} - \mathrm{Liver}_{\mathrm{pre}}\right)/\left(\mathrm{Aorta}_{\mathrm{EP}} - \mathrm{Aorta}_{\mathrm{pre}}\right) \times (1 - \mathrm{hematocrit}),$$

where $\mathrm{Liver}_{\mathrm{EP}}$ refers to iodine measurement from the liver on equilibrium phase images, $\mathrm{Liver}_{\mathrm{pre}}$ refers to iodine

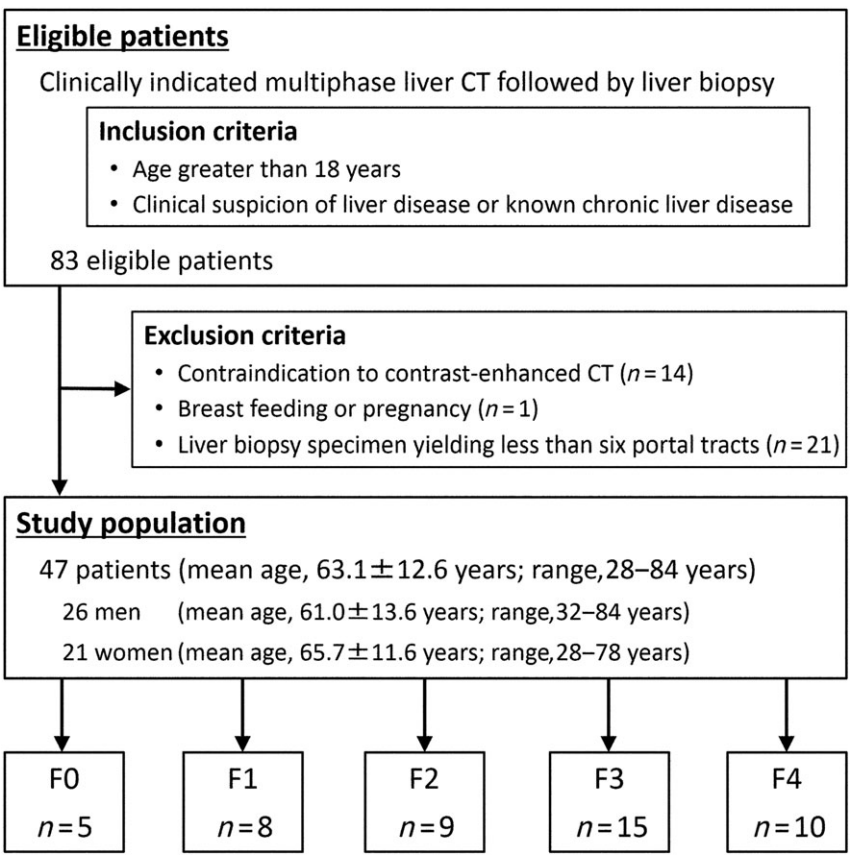

Figure 2 Flowchart of prospective patient accrual process to assess the staging of liver fibrosis in patients with chronic liver disease using dual-energy computed tomography (CT).

Table 1 Demographics and clinical data of 47 patients with chronic liver disease

Parameter	Value
Gender	
Men	26 (55.3)
Women	21 (44.7)
Age, years	
Mean ± SD (range)	63.1 ± 12.6 (28–84)
Body weight, kg	
Mean ± SD (range)	60.5 ± 11.7 (43.0–80.0)
Body mass index	
Mean ± SD (range)	23.7 ± 4.1 (15.7–38.1)
Hematocrit level	
Mean ± SD (range)	0.403 ± 0.042 (0.322–0.503)
Child–Pugh classification	
A	21 (44.7)
B	16 (34.0)
C	10 (21.3)
METAVIR fibrosis stage	
F0	5 (10.7)
F1	8 (17.0)
F2	9 (19.1)
F3	15 (31.9)
F4	10 (21.3)
METAVIR activity grade	
A0	6 (12.8)
A1	14 (29.8)
A2	23 (48.9)
A3	4 (8.5)
Cause of chronic liver disease	
Hepatitis C infection	28 (59.5)
Hepatitis B infection	9 (19.1)
Alcoholic hepatitis	2 (4.3)
Primary biliary cirrhosis	2 (4.3)
Cryptogenic cirrhosis	6 (12.8)

Data are summarized as mean ± standard deviation (SD) for continuous variables, or as counts (percentage) for categorical variables.

measurement from the liver on non-contrast images, $Aorta_{EP}$ refers to iodine measurement from the aorta on equilibrium phase images, and $Aorta_{pre}$ refers to iodine measurement from the aorta on non-contrast images.

Statistical analysis

Continuous variables were expressed as mean ± standard deviation, and categorical variables were summarized as frequencies and percentages. Interobserver agreement in measured iodine densities between the two readers was assessed by using an intraclass correlation coefficient (ICC; two-way mixed model) with 95% confidence interval (CI), which was calculated with a variance component analysis.

Each of the four parameters to estimate iodine uptake of the liver from iodine density measurements were compared among the METAVIR fibrosis stages using the Kruskal–Wallis non-parametric ANOVA test. Spearman's rank correlation coefficients were used to assess the correlations between the calculated values and the METAVIR fibrosis stage. The diagnostic performances of the calculated parameters for staging liver fibrosis were evaluated by using receiver operating characteristic (ROC) curve analysis, and area under the ROC curve (A_z) was calculated. The optimized thresholds were obtained utilizing the maximized Youden index method on ROC analysis. The sensitivity, specificity, positive predictive value, negative predictive value, and accuracy with corresponding 95% CIs were calculated.

A multivariate linear regression analysis with stepwise selection of variables was carried out to evaluate the influence of possible confounding factors associated with each of the two parameters of iodine uptake of the liver (Δ Liver and Δ Liver/Aorta). Independent variables included METAVIR fibrosis stage, METAVIR necroinflammatory

Table 2 Iodine density measurements in 47 patients with chronic liver disease and interobserver agreement

Parameter	Non-contrast	Arterial phase	Portal venous phase	Equilibrium phase
Liver				
Iodine density (mg/cm^3) (range)	4.56 ± 1.54 (1.46–7.00)	17.33 ± 5.51 (6.33–29.38)	32.00 ± 4.44 (22.21–41.21)	24.68 ± 3.81 (17.09–32.89)
ICC (95% CI)	0.951 (0.903–0.989)	0.942 (0.899–0.965)	0.974 (0.965–0.990)	0.972 (0.934–0.994)
Aorta				
Iodine density (mg/cm^3) (range)	6.31 ± 1.56 (3.45–10.14)	139.41 ± 35.04 (68.40–223.74)	65.15 ± 9.12 (43.60–83.05)	47.84 ± 7.16 (31.63–61.92)
ICC (95% CI)	0.955 (0.926–0.984)	0.965 (0.912–0.994)	0.980 (0.947–0.998)	0.987 (0.970–0.992)

Data are summarized as mean ± standard deviation for iodine densities.
CI, confidence interval; ICC, intraclass correlation coefficient.

activity grade, gender, age, body weight, body mass index, and hematocrit level. In this model, independent variables with the least significance were sequentially eliminated from the model if their associated *P*-value was >0.2, and previously eliminated variables could re-enter the model if their *P*-value was <0.5. The coefficient of determination (R^2) was calculated to indicate how well data fitted the statistical model, and ANOVA was used to assess the significance of the model.

For all statistical analyses, reported *P*-values were two-sided, and *P*-values <0.05 were statistically significant. All statistical analyses were undertaken using statistical software SPSS version 20.0 (SPSS, IBM, Chicago, IL, USA).

RESULTS

Study cohort

FORTY-SEVEN PATIENTS (MEAN age, 63.1 ± 12.6 years; age range, 28–84 years) represented the final study cohort (Fig. 2), which included 26 men (mean age, 61.0 ± 13.6 years; range, 32–84 years) and 21 women (mean age, 65.7 ± 11.6 years; range, 28–78 years). The etiology of chronic liver disease in enrolled patients was as follows: hepatitis C infection (*n* = 28), hepatitis B infection (*n* = 9), alcoholic hepatitis (*n* = 2), primary biliary cirrhosis (*n* = 2), and cryptogenic cirrhosis (*n* = 6). The median interval between dual-energy CT of the liver and biopsy was 23 days (interquartile range, 6–43 days). No patient had ascites on CT. The pathological stages of liver fibrosis were F0 in 5 patients, F1 in 8, F2 in 9, F3 in 15, and F4 in 10 (Table 1).

Iodine density measurements and interobserver agreement

Iodine density values from liver and aorta are supplied in Table 2. An excellent agreement in measured iodine densities was found between the two readers (ICC, 0.848–0.957).

Accuracy of iodine density measurements in liver fibrosis staging

Δ Liver/Aorta significantly increased with higher stages of liver fibrosis ($P < 0.001$), whereas no significant correlation was observed between Δ Liver and liver fibrosis stage ($P = 0.650$) (Fig. 3). Δ Liver/Aorta ($\rho = 0.645$, $P < 0.001$) showed good correlation with METAVIR liver fibrosis score, whereas Δ Liver ($\rho = 0.163$, $P = 0.262$) weakly correlated with METAVIR fibrosis stage (Fig. 4).

The area under the ROC curve (A_z) values for assignment of each METAVIR fibrosis stage ranged from 0.795 to 0.855 for Δ Liver/Aorta (Fig. 5). The optimal cut-off values at the intersection of predictive power for Δ Liver/Aorta yielded good discrimination of METAVIR fibrosis stages of ≥F1, ≥F2, ≥F3, and =F4 (Table 3).

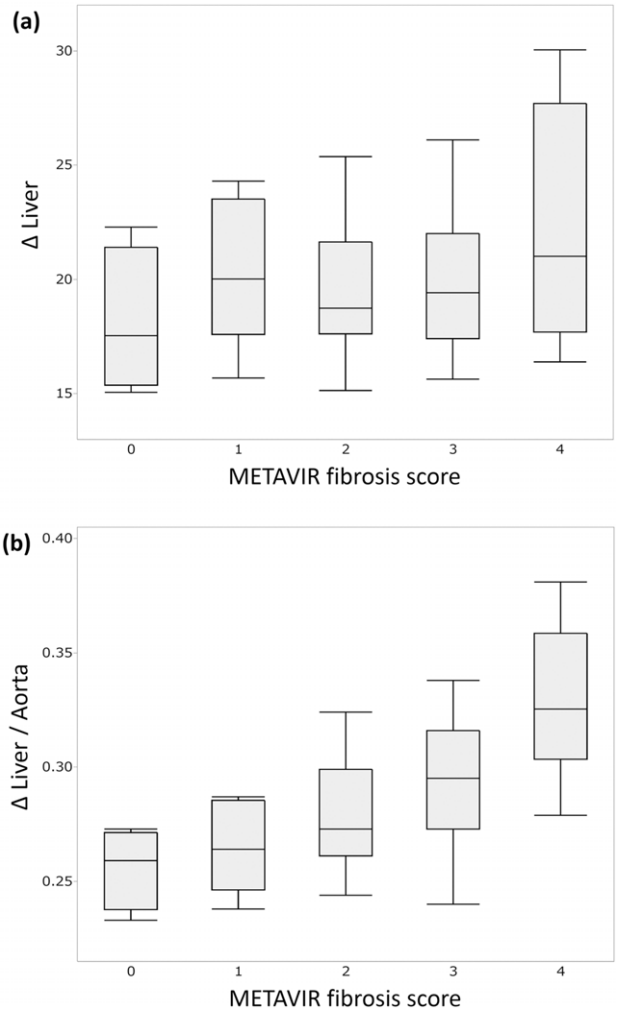

Figure 3 Box plots of iodine uptake of the liver (Δ Liver) (a), representing the difference in iodine density between equilibrium phase and non-contrast images, normalized by aorta (Δ Liver/Aorta) (b) for each METAVIR fibrosis stage in patients with chronic liver disease. Lower boundary of boxes indicates 25th percentile, line within boxes indicates median, and higher boundary of boxes indicates 75th percentile. Error bars indicate smallest and largest values within 1.5 box lengths of 25th and 75th percentiles.

Impact of patient-related factors on iodine density measurements

Multivariate linear regression analyses showed that the METAVIR fibrosis stage was the most significant independent factor associated with Δ Liver/Aorta ($P < 0.001$)

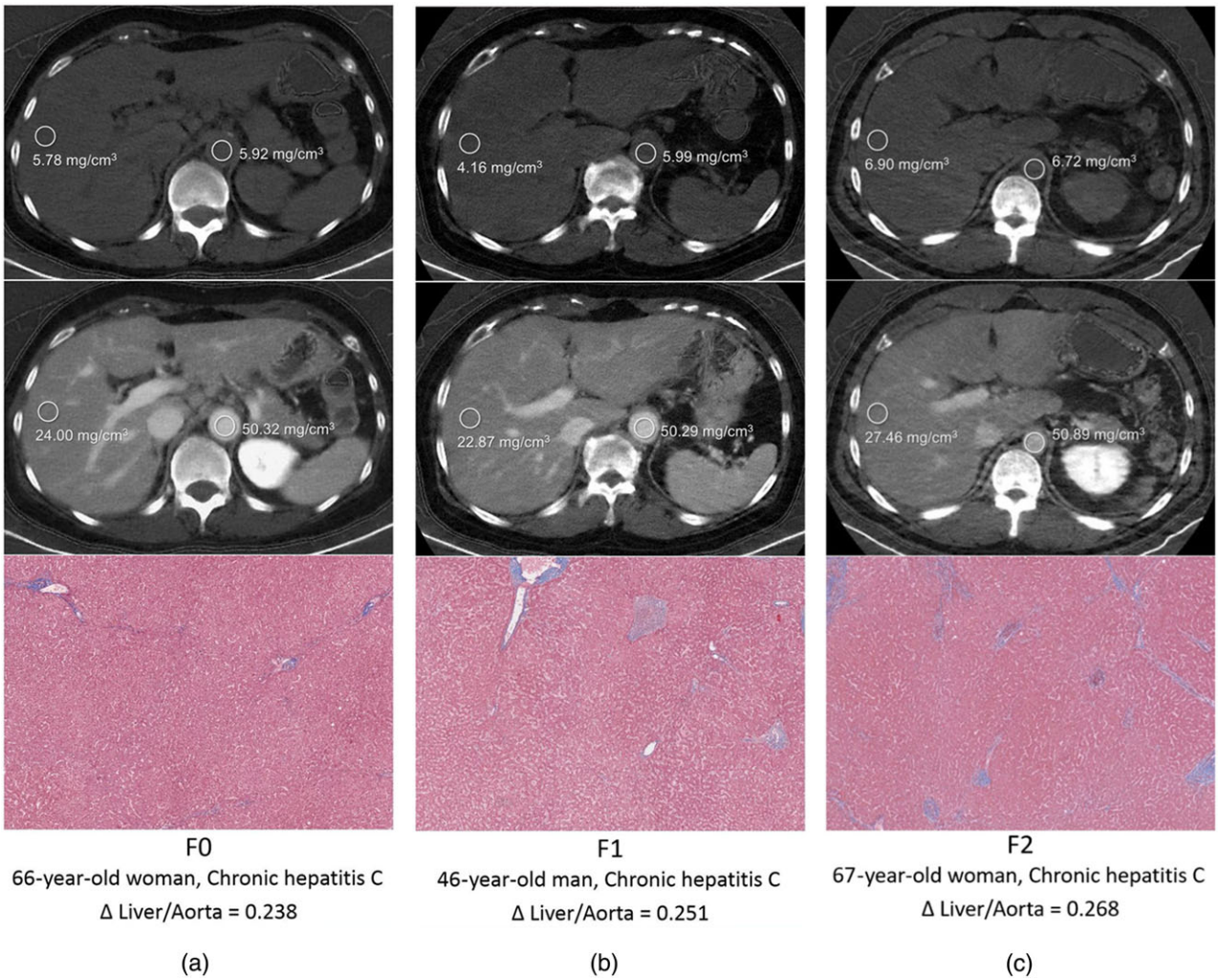

Figure 4 Dual-energy iodine density images from non-contrast and equilibrium phase acquisitions obtained from patients with various liver fibrosis grades (F0–F4), with corresponding Masson trichrome-stained histologic slices. Δ Liver/Aorta, iodine uptake of the liver, normalized by aorta. [Color figure can be viewed at wileyonlinelibrary.com]

(Table 4). Patient body weight had a significant impact on Δ Liver values for estimation of liver fibrosis stage ($P = 0.026$). Other patient-related variables, including METAVIR activity grade, did not have a significant effect on dual-energy density measurements.

DISCUSSION

OUR STUDY RESULTS show that iodine density measurements from contrast-enhanced dual-energy data can non-invasively stage liver fibrosis. Of note, measurements of liver iodine uptake normalized by those of aorta yielded high correlation with METAVIR liver fibrosis stage.

In our study, we used iodine uptake – namely, the difference in iodine density values between equilibrium phase and non-contrast images – rather than iodine density measurements from equilibrium phase images only. This choice depended on our empirical observation that non-contrast iodine density value of the liver was 4.56 ± 1.54 mg/cm^3. Therefore, estimation of hepatic parenchymal fibrosis based only on equilibrium phase data would have failed to fully capture dynamics in iodine distribution within the extracellular space after contrast administration. One possible explanation for non-contrast iodine density values being higher than zero is that a two-material decomposition algorithm, which relies on material basis pairs (i.e., iodine and water), was used in

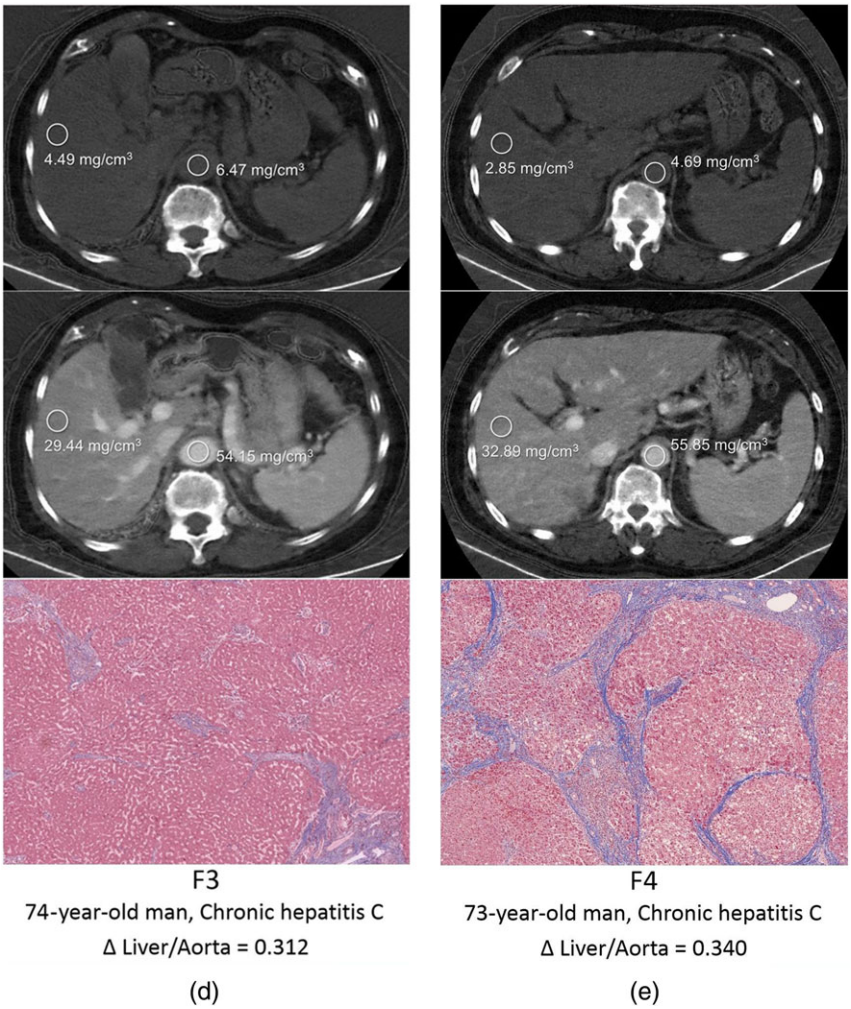

Figure 4 (Continued)

our study. While calculated projections refer to densities of a scanned object ideally composed of iodine and water only, mass attenuation coefficients of liver parenchyma and soft-tissues differ from, and are higher than, that of water.[24,25]

The liver tissue is generally composed of three distinct spaces: intravascular, intracellular, and extravascular/extracellular spaces.[26] During the equilibrium phase, concentration of contrast agent within the intravascular space is approximately equal to that within the extravascular/extracellular space, thus normalization by the vessels has been thought to represent a reasonable method for quantification of iodine concentration in liver interstitial spaces.[12–14] The poor diagnostic performance of Δ Liver might be because this parameter accounts for retention of contrast agent within the intravascular space and the extravascular/extracellular space, whereas Δ Liver/Aorta emphasizes iodine retention within the extravascular/extracellular space, owing to the normalization by the aorta. Our results for correlation between hepatic ECV fraction and histopathological fibrosis stage were higher than those for previous research efforts estimating liver fibrosis using hepatic ECV fraction from contrast-enhanced equilibrium phase CT images.[13,14] This improved correlation might be because iodine density measurements from dual-energy CT more accurately capture iodine retention within the liver parenchyma compared with conventional CT images. Zissen *et al.* reported an A_z value of 0.953 for the prediction of liver cirrhosis.[12] However, we could not compare these results with ours, as their patient cohort included a significant number (33%) of patients without any chronic liver disease and their criteria adopted only the clinical diagnosis of cirrhosis based on review of the medical record and morphological imaging findings,

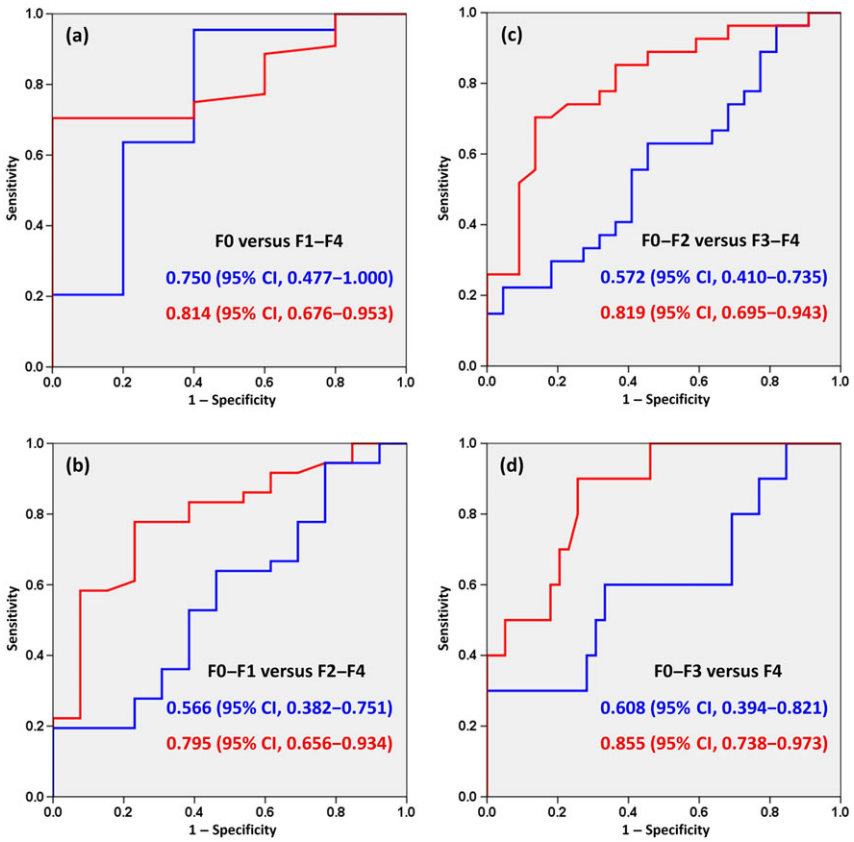

Figure 5 Receiver operating characteristic curves for iodine uptake of the liver (Δ Liver; blue) and Δ Liver normalized to aorta (Δ Liver/Aorta; red) at METAVIR fibrosis score thresholds of ≥F1 (a), ≥F2 (b), ≥F3 (c), and =F4 (d). CI, confidence interval. [Color figure can be viewed at wileyonlinelibrary.com]

Table 3 Optimal cut-off values and predictive power of iodine uptake of the liver, normalized by aorta (Δ Liver/Aorta), for staging liver fibrosis in patients with chronic liver disease

Parameter	≥F1	≥F2	≥F3	=F4
Δ Liver/Aorta				
Cut-off value	0.270	0.274	0.286	0.299
Sensitivity, %	71.4 (66.6–71.4)	79.4 (70.8–84.8)	76.0 (63.3–84.4)	90.0 (63.6–98.2)
Specificity, %	100 (59.5–100)	76.9 (54.5–90.9)	81.8 (67.3–91.3)	73.0 (65.8–75.2)
PPV, %	100 (93.3–100)	90.0 (80.3–96.1)	82.6 (68.8–91.7)	47.4 (33.5–51.7)
NPV, %	29.4 (10.8–29.4)	58.8 (41.7–69.5)	75.0 (61.7–83.7)	96.4 (87.0–99.3)
Accuracy, %	74.5 (65.9–74.5)	78.7 (66.3–86.5)	78.7 (65.2–87.6)	76.6 (65.4–80.1)

Numbers in parentheses are 95% confidence intervals.
NPV, negative predictive value; PPV, positive predictive value.

rather than histological fibrosis stage. In addition, two recent reports have examined hepatic ECV fraction by using the 180-s delay equilibrium phase for staging liver fibrosis.[14,15] Yoon *et al.* indicated that calculation of ECV fraction from routine multiphasic liver CT was feasible in 95.7% (135/141) of the patients by comparing attenuation differences between aorta and portal vein on equilibrium phase images.[14] However, there have been no studies to investigate the validity of 180-s delayed equilibrium phase images for the calculation of hepatic ECV fraction by comparison with longer delayed phase images. Further comparative studies are warranted.

Table 4 Multivariate linear regression models with stepwise method for factors associated with iodine density for staging liver fibrosis in patients with chronic liver disease

Parameter	Coefficient	Standard error	β	*t*-value	VIF	*P*-value
Δ Liver						
Fibrosis score	0.618 (0.200–1.036)	0.208	0.397	2.97	1.071	0.005*
Activity grade	–	–	−0.071	−0.556	1.120	0.581
Gender	–	–	0.228	1.916	1.039	0.062
Age	–	–	0.071	0.581	1.010	0.564
Weight	−0.052 (−0.098 to −0.007)	0.023	−0.335	−2.302	1.272	0.026*
Body mass index	–	–	0.148	0.700	3.060	0.488
Hematocrit	–	–	0.232	1.646	1.197	0.107
Δ Liver/Aorta						
Fibrosis score	0.017 (0.010–0.024)	0.004	0.572	4.782	1.000	<0.001*
Activity grade	–	–	0.044	0.360	1.012	0.721
Gender	–	–	0.083	0.689	1.006	0.494
Age	–	–	−0.120	−0.999	1.008	0.323
Weight	–	–	0.207	1.732	1.043	0.090
Body mass index	–	–	0.106	0.820	1.160	0.416
Hematocrit	–	–	0.051	0.419	1.004	0.677

*Statistically significant value.
Numbers in parentheses are 95% confidence intervals.
Coefficient of determination and ANOVA were: Δ Liver ($R^2 = 0.318$, $P = 0.007$) and Δ Liver/Aorta ($R^2 = 0.327$, $P < 0.001$).
β, standardized coefficient; VIF, variance inflation factor.

The results of our multivariate linear regression analysis, aimed to assess the potential impact of patient-related confounders, showed that only patient body weight had a significant effect on accuracy of dual-energy staging of liver fibrosis. This effect can be explained considering the more pronounced beam-hardening phenomena affecting the low-energy spectrum with larger patient body weight.[27,28] It remains to be further ascertained whether, and to what extent, this interaction can affect the precision and accuracy of the newly proposed technique.

Our data could potentially have important clinical implications. Use of dual-energy iodine measurements might prove useful for non-invasive clinical monitoring of disease progression and treatment response in patients with chronic liver diseases, potentially helping to reduce the need for percutaneous core biopsy. Inevitably, US or MR elastography have substantial advantages for the evaluation of staging liver fibrosis.[8,9] A possible advantage of implementation of dual-energy iodine density measurements is the potential to yield a seamless and non-invasive staging of liver fibrosis into routine multiphasic liver CT protocols undertaken for hepatocellular carcinoma surveillance, without lengthening the acquisition protocol or scanner usage time.[12,13] Another advantage of iodine density measurements is that it does not require dedicated hardware and software unlike US/MR elastography.

Our study had notable limitations. First, although prospectively designed, our research is limited by the relatively small sample size and number of patients for each METAVIR fibrosis stage. A second limitation is the use of liver biopsy as the reference standard, which could have been affected by variability in sampling. Although we attempted to obtain dual-energy iodine density measurements of the liver in the same region where biopsy specimens were attained, there remains considerable potential for spatial misregistration between the two approaches. Third, there was heterogeneity in primary chronic liver disease etiologies in our study. Although it could be argued that histopathologic patterns and spatial distribution of parenchymal fibrosis vary among different liver diseases,[29] the degree of iodine retention could be independent of the type of primary liver damage. Fourth, our investigational approach did not account for steatosis and iron accumulation, which can potentially impact and confound dual-energy iodine density measurements. Incorporation of newly developed multimaterial decomposition algorithms represents a possible strategy to address the impact of these confounders[24,25,30] and future investigation is warranted. Finally, considering the emerging discrepancies and variability in quantification properties among different dual-energy CT hardware implementations,[16–18,31] it must be ascertained whether, and to what extent, our data can be extended to other dual-energy CT systems.

In conclusion, our study results show that iodine density measurements from contrast-enhanced dual-energy data can non-invasively stage liver fibrosis during multiphase CT liver protocols. Clinical implementation of dual-energy iodine measurements of liver fibrosis could prove useful for monitoring disease progression and response to treatment, potentially reducing the need for liver biopsy.

REFERENCES

1 Setiawan VW, Stram DO, Porcel J, Lu SC, Le Marchand L, Noureddin M. Prevalence of chronic liver disease and cirrhosis by underlying cause in understudied ethnic groups: the multiethnic cohort. *Hepatology* 2016; **64**: 1969–77.
2 Friedman SL. Mechanisms of hepatic fibrogenesis. *Gastroenterology* 2008; **134**: 1655–69.
3 Tsochatzis EA, Bosch J, Burroughs AK. Liver cirrhosis. *Lancet* 2014; **383**: 1749–61.
4 Sofue K, Tsurusaki M, Kawasaki R, Fujii M, Sugimura K. Evaluation of hypervascular hepatocellular carcinoma in cirrhotic liver: comparison of different concentrations of contrast material with multi-detector row helical CT – a prospective randomized study. *Eur J Radiol* 2011; **80**: e237–e242.
5 Regev A, Berho M, Jeffers LJ *et al.* Sampling error and intraobserver variation in liver biopsy in patients with chronic HCV infection. *AJR Am J Roentgenol* 2002; **97**: 2614–8.
6 Rousselet MC, Michalak S, Dupre F *et al.* Sources of variability in histological scoring of chronic viral hepatitis. *Hepatology* 2005; **41**: 257–64.
7 Schiano TD, Azeem S, Bodian CA *et al.* Importance of specimen size in accurate needle liver biopsy evaluation of patients with chronic hepatitis C. *Clin Gastroenterol Hepatol* 2005; **3**: 930–5.
8 Yoon JH, Lee JM, Joo I *et al.* Hepatic fibrosis: prospective comparison of MR elastography and US shear-wave elastography for evaluation. *Radiology* 2014; **273**: 772–82.
9 Tang A, Cloutier G, Szeverenyi NM, Sirlin CB. Ultrasound elastography and MR elastography for assessing liver fibrosis: part 2, diagnostic performance, confounders, and future directions. *AJR Am J Roentgenol* 2015; **205**: 33–40.
10 Feier D, Balassy C, Bastati N, Stift J, Badea R, Ba-Ssalamah A. Liver fibrosis: histopathologic and biochemical influences on diagnostic efficacy of hepatobiliary contrast-enhanced MR imaging in staging. *Radiology* 2013; **269**: 460–8.
11 Smith AD, Branch CR, Zand K *et al.* Liver surface nodularity quantification from routine CT images as a biomarker for detection and evaluation of cirrhosis. *Radiology* 2016; **280**: 771–81.
12 Zissen MH, Wang ZJ, Yee J, Aslam R, Monto A, Yeh BM. Contrast-enhanced CT quantification of the hepatic fractional extracellular space: correlation with diffuse liver disease severity. *AJR Am J Roentgenol* 2013; **201**: 1204–10.
13 Bandula S, Punwani S, Rosenberg WM *et al.* Equilibrium contrast-enhanced CT imaging to evaluate hepatic fibrosis: initial validation by comparison with histopathologic sampling. *Radiology* 2015; **275**: 136–43.
14 Yoon JH, Lee JM, Klotz E *et al.* Estimation of hepatic extracellular volume fraction using multiphasic liver computed tomography for hepatic fibrosis grading. *Invest Radiol* 2015; **50**: 290–6.
15 Guo SL, Su LN, Zhai YN *et al.* The clinical value of hepatic extracellular volume fraction using routine multiphasic contrast-enhanced liver CT for staging liver fibrosis. *Clin Radiol* 2017; **72**: 242–6.
16 Heye T, Nelson RC, Ho LM, Marin D, Boll DT. Dual-energy CT applications in the abdomen. *AJR Am J Roentgenol* 2012; **199**: S64–S70.
17 Marin D, Boll DT, Mileto A, Nelson RC. State of the art: dual-energy CT of the abdomen. *Radiology* 2014; **271**: 327–42.
18 Mileto A, Sofue K, Marin D. Imaging the renal lesion with dual-energy multidetector CT and multi-energy applications in clinical practice: what can it truly do for you? *Eur Radiol* 2016; **26**: 3677–90.
19 Kaza RK, Caoili EM, Cohan RH, Platt JF. Distinguishing enhancing from nonenhancing renal lesions with fast kilovoltage-switching dual-energy CT. *AJR Am J Roentgenol* 2011; **197**: 1375–81.
20 Potretzke TA, Brace CL, Lubner MG, Sampson LA, Willey BJ, Lee FT Jr. Early small-bowel ischemia: dual-energy CT improves conspicuity compared with conventional CT in a swine model. *Radiology* 2015; **275**: 119–26.
21 Mileto A, Nelson RC, Marin D, Roy Choudhury K, Ho LM. Dual-energy multidetector CT for the characterization of incidental adrenal nodules: diagnostic performance of contrast-enhanced material density analysis. *Radiology* 2015; **274**: 445–54.
22 Bedossa P, Poynard T. An algorithm for the grading of activity in chronic hepatitis C. The METAVIR Cooperative Study Group. *Hepatology* 1996; **24**: 289–93.
23 Van Beers BE, Materne R, Annet L *et al.* Capillarization of the sinusoids in liver fibrosis: noninvasive assessment with contrast-enhanced MRI in the rabbit. *Magn Reson Med* 2003; **49**: 692–9.
24 Liu X, Yu L, Primak AN, McCollough CH. Quantitative imaging of element composition and mass fraction using dual-energy CT: three-material decomposition. *Med Phys* 2009; **36**: 1602–9.
25 Mendonca PR, Lamb P, Sahani DV. A flexible method for multi-material decomposition of dual-energy CT images. *IEEE Trans Med Imaging* 2014; **33**: 99–116.
26 Villeneuve JP, Dagenais M, Huet PM, Roy A, Lapointe R, Marleau D. The hepatic microcirculation in the isolated perfused human liver. *Hepatology* 1996; **23**: 24–31.
27 Marin D, Pratts-Emanuelli JJ, Mileto A *et al.* Interdependencies of acquisition, detection, and reconstruction techniques on the accuracy of iodine quantification in varying patient sizes employing dual-energy CT. *Eur Radiol* 2015; **25**: 679–86.
28 Feuerlein S, Heye TJ, Bashir MR, Boll DT. Iodine quantification using dual-energy multidetector computed tomography

imaging: phantom study assessing the impact of iterative reconstruction schemes and patient habitus on accuracy. *Invest Radiol* 2012; **47**: 656–61.
29 Sturm N, Marlu A, Arvers P, Zarski JP, Leroy V. Comparative assessment of liver fibrosis by computerized morphometry in naive patients with chronic hepatitis B and C. *Liver Int* 2013; **33**: 428–38.
30 Lamb P, Sahani DV, Fuentes-Orrego JM, Patino M, Ghosh A, Mendonca PR. Stratification of patients with liver fibrosis using dual-energy CT. *IEEE Trans Med Imaging* 2015; **34**: 807–15.
31 Mileto A, Barina A, Marin D *et al*. Virtual monochromatic images from dual-energy multidetector CT: variance in CT numbers from the same lesion between single-source projection-based and dual-source image-based implementations. *Radiology* 2016; **279**: 269–77.